 doi:10.20944/preprints202206.0277.v1

Article

Fuzzy Artificial Intelligence Based Control Strategy Applied to an Electromagnetic Frequency Regulator in Wind Generation Systems

Daniel C. C. Crisóstomo [1,†], Thiago F. do Nascimento [2,†], Evandro A. D. F. Nunes [3,†], Elmer R. L. Villarreal [4,†,*], Ricardo F. Pinheiro [2,†] and Andrés O. Salazar [2,†]

[1] Department of Sciences and Technology, Federal Rural University of Semi-arid (DCT-UFERSA), Caraúbas 59780-000, Brazil; daniel.crisostomo@ufersa.edu.br
[2] Department of Computer Engineering and Automation, Federal University of Rio Grande do Norte (DCA-UFRN), Natal 59072-970, Brazil; thiago.figueiredo@ufrn.br ; andres@dca.ufrn.br ; ricardo.pinheiro@ufrn.br
[3] The Federal Institute of Education, Science and Technology of Bahia (IFBA), Salvador, 40301-015, Brazil; evandro.nunes@ifba.edu.br
[4] Department of Natural Sciences, Mathematics, and Statistics, Federal Rural University of Semi-arid (DCME-UFERSA), Mossoró 59625-900, Brazil; elmerllanos@ufersa.edu.br
* Correspondence: elmerllanos@ufersa.edu.br
† These authors contributed equally to this work.

Abstract: This paper presents the implementation of a control strategy based on fuzzy logic artificial intelligence (AI) for speed regulation of an electromagnetic frequency regulator (EFR) prototype, aiming to eliminate the dependence on knowledge of physical parameters in the most diverse operating conditions. Speed multiplication is one of the most important steps in power generation wind. Gearboxes are generally used for this purpose. However, they have a reduced lifespan and a high failure rate and are still noise sources. The search for new ways to match the speed (and torque) between the turbine and the generator is an important research area to increase the energy, financial and environmental efficiency of wind systems. The EFR device is an example of an alternative technology that this team of researchers has proposed. It counts the fact of taking advantage of the main advantages of an induction machine with the rotor in a squirrel cage positively. In the first studies, the EFR control strategy consisted of the conventional PID controllers, which has several limitations widely discussed in the literature. This strategy also limits the EFR's performance, considering its entire operating range. The simulation program was developed using the Matlab/Simulink platform, while the experimental results were obtained in the laboratory emulating the EFR-based system. The EFR prototype used has 2 poles, a nominal power of 2.2 kW, and a nominal frequency of 60 Hz. Experimental results were presented to validate the efficiency of the proposed control strategy.

Keywords: Speed control; Fuzzy Controller; Electromagnetic Frequency Regulator ; Wind Energy; Photovoltaics

1. Introduction

Due to environmental issues, electricity generation systems using wind energy have increased rapidly all over the world. However, the variation in wind speed is the main problem for this type of system. Considering the wide range of wind variations and taking into account that turbine torque and power are very sensitive to such variations (torque varies as the square and power as the cube of wind speed), wind turbines are oversized concerning the energy they actually produce over time, which is characterized by the capacity factor. In addition, the need to expand the generation capacity has led to turbines being dimensioned with increasingly larger diameters, which increases the torque produced on the turbine shaft and reduces the permissible speed at the blade tip. Thus, a speed multiplier is used in many of the technologies in use to match the wind turbine and the electric generator speeds [1].

Currently, speed multipliers are the main cause of noise in wind turbines. In addition, they are the equipment that most require maintenance and replacement in a wind power system [2], [3] , [4] and have a very short lifespan when compared to other elements of a wind generation system [5], [6]. On the other hand, conventional wind systems are connected to the electrical power system (EPS) through power electronic devices, which can contribute to the increase of voltage and current harmonic distortion at the point of common coupling (PCC) of the system AC, whose intensity needs to be limited [7]. In order to overcome these limitations, the line of research that deals with the EFR stand out, which is defined as a device consisting of an induction machine with adaptations [8]. Among the main objectives of the EFR are:

- Contribute to the reduction of mechanical impacts that shorten the useful life of the speed multiplier;
- Reduce disturbances in active and reactive power and harmonics caused by connecting electronic converters in the interconnection of wind turbines, photovoltaic systems, or other forms of generation with the electrical grid;
- To provide an alternative for the hybridization of renewable, intermittent energy sources, whose synergy, under adequate dimensioning, allows the generation of firm energy, regardless of the climatic conditions of each moment;
- Enable distributed generation systems from intermittent renewable sources, which can operate in isolation from the electricity grid, ensuring full service to demand with a high level in relation to the quality of the energy supplied.

In recent years, some works related to the application and control of the EFR device have been proposed in the literature [8] to [14]. In order to increase the reliability and efficiency of the wind generation system, the replacement of the speed multiplied by the EFR was proposed in [8], [9], [10]. In these works, it was installed between the wind turbine and a synchronous generator connected to the electrical grid. In this case, the main objective was to ensure that the EFR's rotor shaft, which was mechanically coupled to the rotor shaft of the synchronous generator, had the necessary rotation speed so that the frequency of the voltage generated was compatible with the electrical grid frequency, regardless of the variation in wind speed. The EFR-based system presented a satisfactory performance for a small range of speeds. However, it did not obtain the same performance in more abrupt variations of the speed reference values. In addition, the system behavior for low values of armature speed, in which wind turbines are usually affected (6-20 rpm), was also not evaluated. In [11], a method was proposed to track the maximum wind power extraction point through the control structure associated with the EFR. In this work, unlike the applications found in the literature, the EFR device was used to drive a squirrel-cage induction generator connected to the electrical network. The system presented a satisfactory performance for large variations in wind speed. Furthermore, as the converter has no connection to the grid, this topology proved to be more effective in withstanding a severe short circuit at the induction generator terminals than a conventional doubly-fed induction generator (DFIG) topology. Subsequently, a power quality analysis applied to the wind generation topology discussed in [11] was proposed by [12]. The authors concluded that the high-frequency components of the voltage generated in an EFR-based system are naturally attenuated by the inertia inherent in the EFR-SCIG mechanical system, which results in an advantage compared to DFIG wind generation and permanent magnet synchronous generator (PMSG) topologies.

The control strategy adopted in the works mentioned above was based on a vector control technique that consists of two cascaded control loops, as discussed in [13]. In addition, the control framework employs standard PI-type controllers. However, the controller design was not presented in these works, making it difficult to adjust the control gains to achieve a desired dynamic response. Thus, a design methodology for a vector control strategy applied to EFR was proposed in [14]. The system controllers were designed

 doi:10.20944/preprints202206.0277.v1

using the root locus method (RLM) and presented dynamic performance compatible with the desired transient response specifications. However, the controllers performance was not evaluated for parametric variation of the system. Thus, a dynamic analysis of the system considering variations in the EFR's parameters was proposed in [15]. The analysis based on transient and steady-state response specifications showed the varying influence of the EFR device parameters on its dynamic behavior. The authors concluded that large parametric variations could result in degradation in the transient response of the system controllers. Consequently, it is necessary to evaluate the dynamic behavior of the EFR operating with more robust control strategies in relation to parametric variations and system disturbances.

2. System Description

Figure 1 presents the EFR Based system block diagram employed for the conducting performance studies. In this configuration, a DC motor is responsible for emulating the kinect energy stored in turbine blades of a wind power system which is then transmitted through the low-speed shaft. DC motor is mechanically coupled to EFR's armature and along this connection it is possible to access its armature phases by slip rings that is fed by means of a three-phase voltage source inverter (VSI) with L-filter. The EFR is the speed conversion stage main device and allows torque transmission to the synchronous generator that supplies energy to a three-phase resistive load.

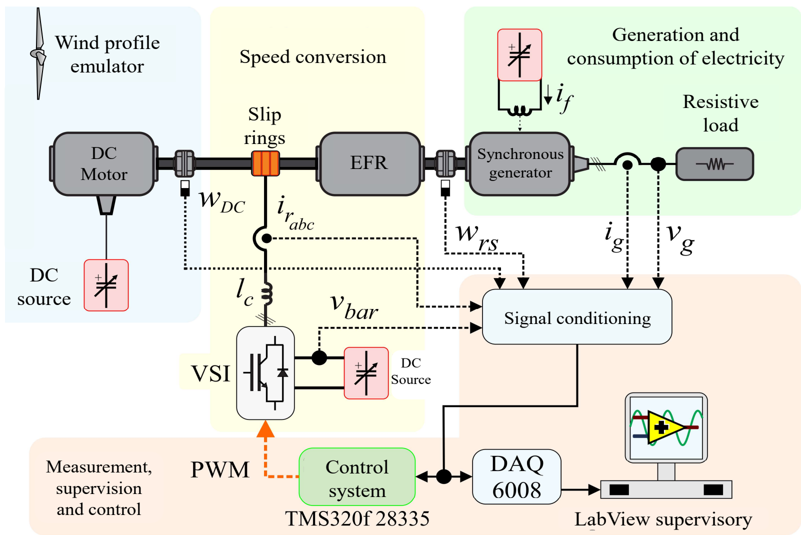

Figure 1. Block Diagram of EFR Based-Wind Power System.

The measurement, supervision and control stage deals with the main system variables such as DC-link voltage (Vbar), EFR's armature currents (Irabc), DC motor (Wdc) and EFR's rotor speed (Wrs), and a single-phase voltage (Vg) and current (Ig) absorbed by the resistive load. These data are sent to a LabView supervisory through a digital acquisition device DAQ 6008 and to the control system that is performed by a Texas Instruments TMS320f28335 which runs the control strategy. In the Table (1), (2) and (3) presents the main specifications of the EFR Based system in Figure 1.

A summary of the most important system parameters in Table (1), (2) and (3).

Preprints (www.preprints.org) | NOT PEER-REVIEWED | Posted: 21 June 2022 doi:10.20944/preprints202206.0277.v1

Table 1. DC Motor Nominal Parameters.

Parameters	Value
Power	1.5 cv
Velocity	1800 rpm
Voltage	180 V
Current	6.0 A

Table 2. EFR Nominal Parameters.

Parameters	Value
Nominal Power	3.0 cv
Nominal Speed	3600 rpm
Number of poles	2
Voltage	180 V
Resistance of rotor and armature	2.3 e 2.8 Ohm
rotor and armature reactance	3.7 e 3.9 Ohm
Mutual Inductance	220 mH

Table 3. Synchronous Generator Nominal Parameters.

Paramaters	Value
Power	1.0 kW
Velocity	1800 rpm
Number of poles	4
Voltage	180 V
Resistance of rotor and armature	1.7 e 4.1 Ohm
Field Resistance and Reactance	1.1 e 2.8 Ohm
Mutual Inductance	300 mH

The EFR constructive aspect is depicted in Figure 2. The armature consists of a conventional induction machine stator with adaptations that enables its rotation by a prime mover, represented, in this work, by the DC motor rotor shaft. The electrical contact at coils of this rotor is carried out by means of slip rings, which allow injection and monitoring of the flowing currents through the EFR armature windings. The rotor consists of a squirrel-cage rotor and its rotation is the EFR's output speed, which in turn drives the synchronous-machine-rotor shaft. The junction and the support of the EFR's rotor with the synchronous generator rotor are carried out using a coupler and mechanical bearing, respectively. Thus, the rotor is responsible for maintaining the voltage and frequency stability of the power supplied to the resistive load. More information about EFR features are found in [9], [10], [15].

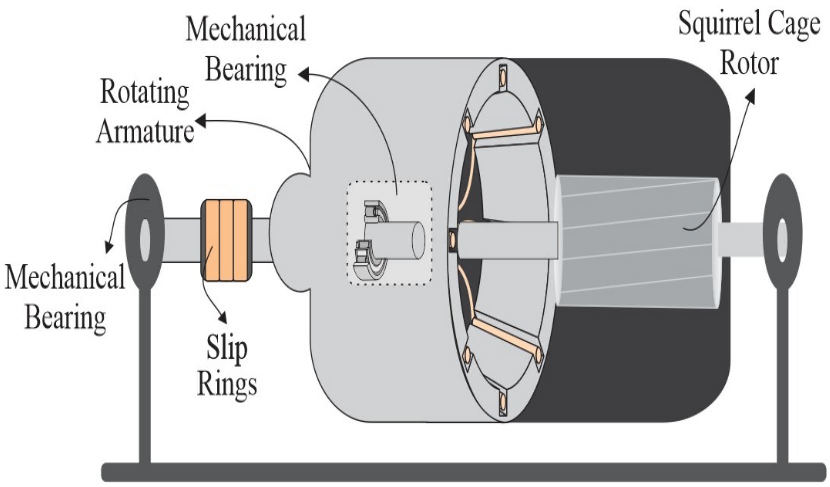

Figure 2. Constructive Aspect of the EFR.

3. EFR Modeling and Simulation

In this section 3 the EFR's model is described, as well as a simulation by numerical computation software for later validation.

3.1. EFR's dynamic model

The dynamic model of the EFR device is based on the model of a squirrel-cage rotor induction machine given by:

$$v_{sd} = R_s i_{sd} + \frac{d\lambda_{sd}}{dt} - \omega_s \lambda_q \quad (1)$$

$$v_{sq} = R_s i_{sq} + \frac{d\lambda_{sq}}{dt} - \omega_s \lambda_d \quad (2)$$

$$\lambda_{sd} = L_s i_{sd} + L_m i_{rd} \quad (3)$$

$$\lambda_{sq} = L_s i_{sq} + L_m i_{rq} \quad (4)$$

$$v_{rd} = R_r i_{rd} + \frac{d\lambda_{rd}}{dt} - (\omega_s - \omega_r)\lambda_{rq} \quad (5)$$

$$v_{rq} = R_r i_{rq} + \frac{d\lambda_{rq}}{dt} - (\omega_s - \omega_r)\lambda_{rd} \quad (6)$$

$$\lambda_{rd} = L_r i_{rd} + L_m i_{sd} \quad (7)$$

$$\lambda_{rq} = L_r i_{rq} + L_m i_{sq} \quad (8)$$

The electromagnetic torque is the variable that works as the connecting link between the electrical and mechanical system of the EFR and can be described by the equation (9). In this equation (9) can be seen that if i_{sd} is kept at zero, the entire electromagnetic torque can only be obtained by regulating i_{sq}.

$$T_{EFR} = p_{efr}(\lambda_{sd} \cdot i_{sq} - \lambda_{sq} \cdot i_{sd}) \quad (9)$$

The equation (10) describes the EFR's mechanical behavior, with J_m, F_m, T_m, ω_r being the moment of inertia of the entire mass connected to the rotor, the friction coefficient of the rotor, the resistant torque of the load coupled to the motor shaft and the angular speed of the rotor.

$$J_m \frac{d\omega_r}{dt} = T_{EFR} - T_m - F_m \omega_r \quad (10)$$

 doi:10.20944/preprints202206.0277.v1

From the prototype constructive aspect with the EFR, it is known that the armature is free to rotate favorable to the movement of the mechanical driving force emulated by the DC motor. Thus, this movement also has a mechanical behavior, as equation (11).

$$J_a \frac{d\omega_{ra}}{dt} = T_v - T_{EFR} - F_a \omega_{ra} \tag{11}$$

Where J_a, F_a, T_v, ω_{ra} represent the inertia moment in the entire connected mass to the armature, the friction coefficient of armature, conjugate imposed by the wind emulation, and the angular velocity of armature. The equations (10) and (11) demonstrate that T_{EFR} performs the intermediate between the speeds of rotor and armature.

3.2. *Model Simulation Validation*

For validation through simulation, the Simulink/Matlab software is used. Initially, the induction machine model is implemented traditionally by the equations (1) to (10). However, incorporating the mechanical behavior of the armature into the model generates an alteration that deserves to be mentioned. The synchronous speed depends only on the frequency of the voltages applied to the machine armature. Thus, the armature angular speed perturbs this variable, increasing or decreasing the rotor's liquid field. So, for this effect is perceived by the rotor, the block diagram, illustrated in Figure 3, is inserted in the induction machine model code. Another change concerns the equations (1), (2), (5), (6), which instead of receiving ω_s directly, now get ω_{sa} on input its blocks, which represents the angular speed resulting from the sum of ω_{ra} and ω_s.

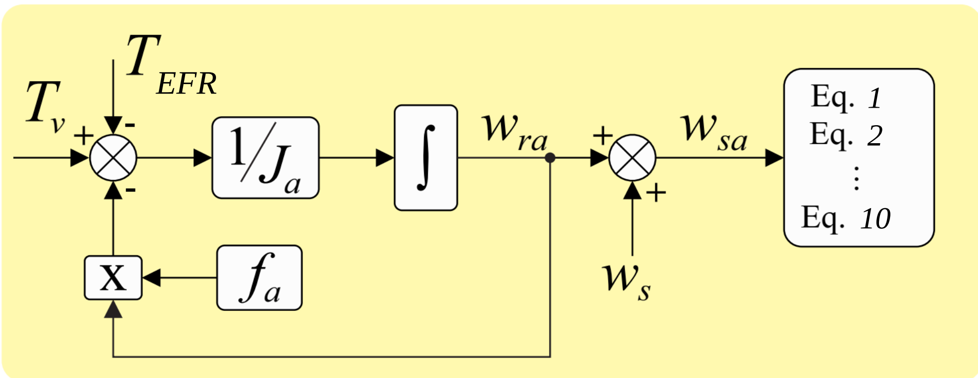

Figure 3. Block diagram of armature speed influence.

Thus, in order to approximate the simulation to the real scenario with the EFR, an induction machine with the same rated power as the EFR and with similar dimensions. The main simulation specifications are summarized in Table 4.

Preprints (www.preprints.org) | NOT PEER-REVIEWED | Posted: 21 June 2022 doi:10.20944/preprints202206.0277.v1

Table 4. Specifications for the simulation of the EFR elementary model.

Parameter	Value
Poles number (P_{efr})	2
Rotor resistance (R_r)	6 Ω
Armature resistance (R_s)	6 Ω
Armature inductance (L_s)	30 mH
Rotor inductance (L_r)	30 mH
Mutual coupling inductance (L_m)	500 mH
Nominal Power (P)	2.0 kW
Nominal Voltage (V_L)	380 V
Nominal Current (I_f)	2.8 A
Nominal frequency	60 Hz
Nominal Velocity	1740 rpm
Inertia Moment (Rotor+Generator) (J_m)	0.02 kg·m
Inertia Moment (Armature+Turbine) (J_a)	0.978 kg·m
Friction coefficient (Rotor+Generator) (F_m)	0.003 N·m/rad·s
Friction coefficient (Rotor+Turbine) (F_a)	9.0 N·m/rad·s

The test for the elementary model validation consists of a direct start of the machine for an analysis period of 5 s, and the results is shown in Figure 4. There is no velocity regulation in this simulated scenario. The rotor speed reaches the nominal value after 0.7 s has elapsed, as illustrated in Figure 4a, while no torque value T_v is imposed on the model, as shown in to Figure 4b. Under these conditions, the EFR's model behaves like a traditional induction motor, with armature inrush currents that reach almost five times the rated current value and with reduced rotor currents for the nominal slip at no load, as shown in Figures 4c and 4d.

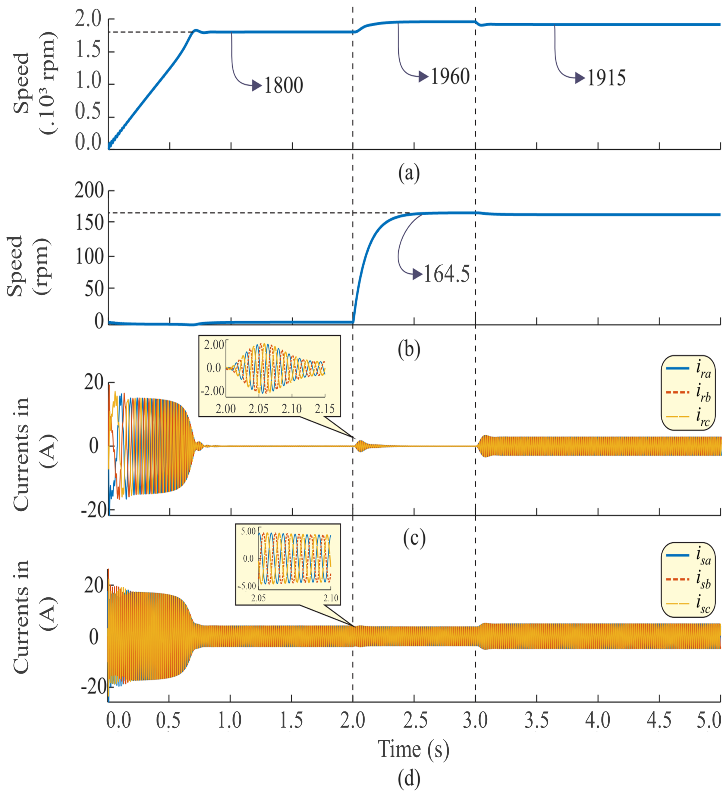

Figure 4. Simulation analysis for the EFR elementary model of EFR (a) Rotor speed, (b) Armature speed, (c) Rotor currents (d) Armature currents

Preprints (www.preprints.org) | NOT PEER-REVIEWED | Posted: 21 June 2022 doi:10.20944/preprints202206.0277.v1

After 2.0 s, the wind emulator starts with a torque T_v equivalent to 300 N. Under these conditions, the resulting armature speed reaches 164.5 rpm. This velocity is transferred to the rotor motion, even with the mains frequency maintained at 60 Hz. Another interesting effect is the effective current consumed reduction by the armature from 2.819 A to 2.653 A, as illustrated in Figure 4d. Meanwhile, the rotor suffers from the synchronous speed increase and the speed of the armature, as the amplitude of the current signals of rotor. Here, it is possible to manage the system's power flow with EFR. As of 3.0 s, a constant torque load equivalent to 5 $N.m$ is entered in the rotor. With this disturbance in the system, it is possible to see that the model remains functional, as it manages to overcome the resistant conjugate with the increase of currents from rotor and armature. There is also a reduction in rotor speed at 45 rpm, which causes an increase in the EFR's slip.

4. Control Strategy

In section is presented aspects related to the EFR-based system control, together with the detailing of the main contribution to speed regulation.

4.1. Rotor Flux Oriented Control

The control strategy initially proposed by [9] consists of an adaptation of the FOC and is illustrated in Figure 5. The estimation of the rotor flux is important to obtain the rotor angle (ρ) that is necessary for the decoupling of the variables that influence the rotor flux (i_{sd}) and also the conjugate (i_{sq}). From these variables, current controllers R_{id}(s) and R_{iq}(s) were used, which initially employ PI-type controllers. These controllers determine the reference voltages ($V^*_{f\ abc}$) that should be applied to the VSI via PWM modulation.

With the measurement of mechanical velocity (w), it is possible to elaborate a control loop responsible for determining the reference torque from the quadrature-axis current ($i^*_{sq_{efr}}$), which is necessary for the system energy balance, which is guaranteed using a speed regulator (R_w) of the PI controller. Due to its direct relationship with the quadrature-axis current, as already determined by [13], the reference current ($i^*_{sq_{efr}}$) plays an important role in the transmission of energy by the EFR through the conjugate (T_{efr}).

For system operation without considerable vibrations and minimal heating losses, it is necessary to adopt a suitable rotor flux. This flux regulation is performed by a PI controller R_ϕ(s) that acts on the direct-axis current ($i^*_{sd_{efr}}$). The dimensioning of controller gains used for the conventional regulation follows the procedures proposed in [13].

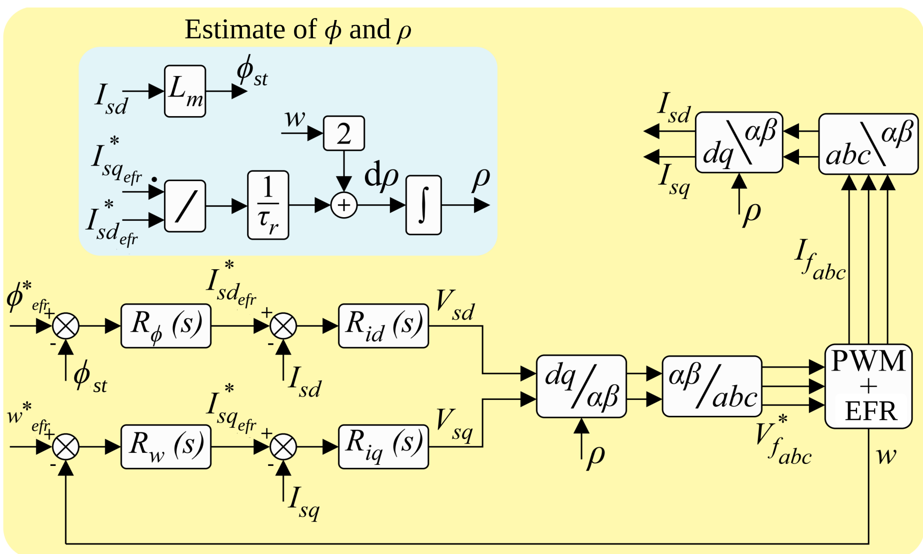

Figure 5. Rotor-flux-oriented control with conventional speed regulation.

 doi:10.20944/preprints202206.0277.v1

4.2. Fuzzy control implementation

An important contribution of this article is the regulation of speed and torque through a Sugeno model Fuzzy-PI controller replacing the PI controller, adopted by [9]. The schematic diagram of the proposed fuzzy speed control is illustrated in Figure 6. Fuzzy controller requires knowledge the error signal and also the error variation to determine the control signal, which must be integrated to represent the reference stream ($i^*_{sq_{efr}}$).

The gains tuning associated with the fuzzy controller was performed according to the procedures available in the works of [17] and [18]. In this controller, three triangular membership functions were considered for the error signal with the following linguistic variables: Negative Error - EN; Zero Error- EZ; Positive Error - EP. In Figure 7, the literal intervals of relevance function to the speed error as a function of its respective universe of discourse. In the figure on screen, the axis that represents the discourse universe is not on a linear scale. For the error derivative, three triangular membership functions were used with the following nomenclatures: Negative Derivative - DN; Derivative Zero - DZ; and Positive Derivative - DP, because in the analysis of the derivative, it is only necessary to evaluate if it increases, remains constant or decreases and, with that, know if the signal is moving away from or approaching the reference. Figure 8 illustrates the ranges of membership functions for the derivative of the velocity error. Once again, the axis that represents the discourse universe is not on a linear scale.

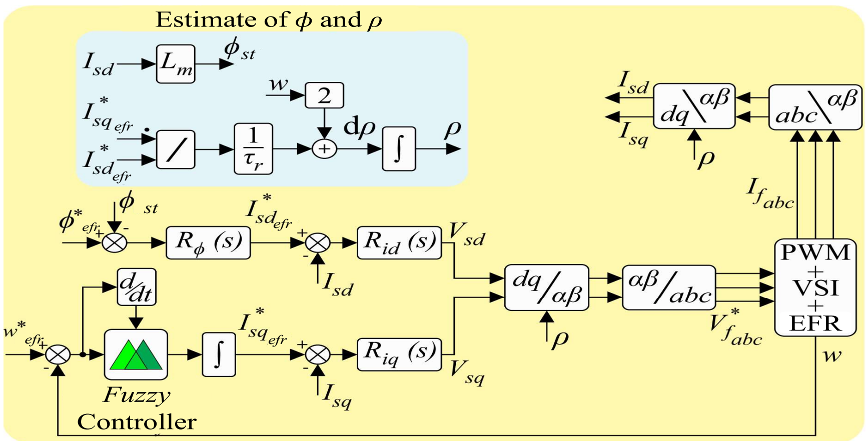

Figure 6. Rotor-flux-oriented control with fuzzy speed regulation.

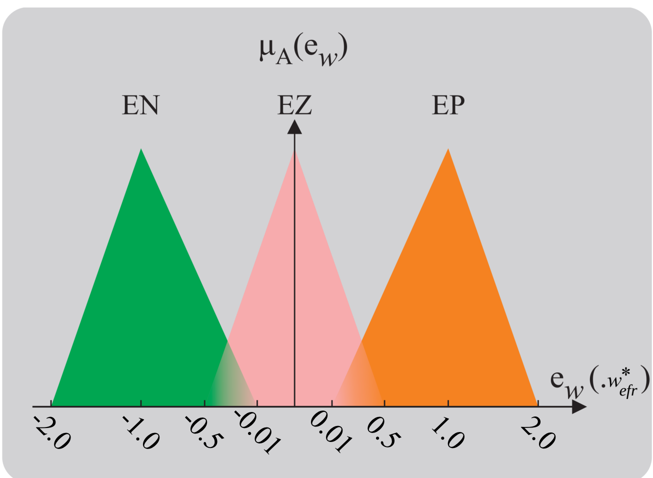

Figure 7. Membership functions associated with the speed error signal.

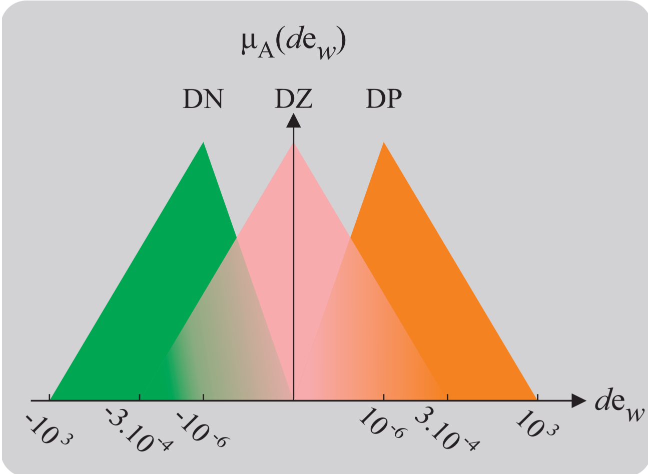

Figure 8. Membership functions associated with the sign of the speed error derivative.

The range used for error signals depends on the imposed reference value to speed control and may consider the possibility of the EFR's operating in both rotation directions with nominal values. As for the error variation of velocity, the polarity of the variation measured by the acquisition system was considered data. Based on this organization, the ranges of membership functions are summarized in the Table (5).

Table 5. Parameters of Membership Functions e_w and de_w.

FP	Parameter	Value	Parameter	Value	Parameter	Value
EN	a_1	$-2\omega^*_{efr}$	b_1	$-\omega^*_{efr}$	c_1	$-0.01\omega^*_{efr}$
EP	a_2	$-0.01\omega^*_{efr}$	b_2	ω^*_{efr}	c_2	$2\omega^*_{efr}$
EZ	a_3	$-0.5\omega^*_{efr}$	b_3	0.0	c_3	$0.5\omega^*_{efr}$
DN	a_4	-1000	b_4	-0.00001	c_4	0.0
DP	a_5	0.0	b_5	0.00001	c_5	1000
DZ	a_6	-0.0003	b_6	0.0	c_6	0.0003

After implementing the controller inputs, it was necessary to design the functions output suggestion for each of the angles, as illustrated in the Table (6). The rules of inference implemented follow the equation (12), with n = 1,2,$\cdots$,9:

$$S_n = K_{p_n}.de_w + K_{in}.e_w + H_0 \tag{12}$$

where H_0 is a homopolar component that can be inserted into the control to compensate for offset values.

Table 6. Fuzzy rules framework for EFR speed regulation.

de_w \ e_w	**EN**	**EZ**	**EP**
DN	S_1	S_2	S_3
DZ	S_4	S_5	S_6
DP	S_7	S_8	S_9

In this section (4), the control characteristics of the generation prototype of wind energy developed in laboratory elucidate the application of the fuzzy controller in the system speed regulation. In addition, the tuning procedure was described in said controller.

 doi:10.20944/preprints202206.0277.v1

5. Experimental Results

The wind power generation prototype evaluation with the EFR regulated by the control strategies presented in the section (5) is based on the transient performance analysis and permanent regimes for different operating scenarios. In this section (5), the details of the tests carried out are described, in addition to discussing and presenting the experimental results regarding the performances obtained for each scenario, together with a comparative analysis between them.

5.1. Description of Operation Scenarios

In this work, the operating scenarios are characterized by synchronous generator mode traction, which can be both no-load and loaded. Both discuss the main differences in performance based on the control strategy adopted. In the first scenario, the generator electrical terminals are disconnected from any element that consumes electrical energy and, therefore, there is no relevant value of current or power electrical system that requires evaluation. From the EFR point of view, active power is expressive only during start-up, as the control must overcome the inertia of an equivalent mass to the sum of the individual masses of the rotor and the electric generator rotor. In the load scenario, two resistors are connected in parallel to each phase of the synchronous generator so that the power to be consumed can exceed 200 W per phase, depending on the field winding excitation circuit. In addition, to the mass of the rotating parts, the existence of a load coupled to the generator synchronous gives rise to a counter-conjugate, proportional to the excitation current I_f in the rotor shaft, and the EFR must compensate for that through its control strategy. For this study, the load is kept constant throughout all scenarios operating under load.

The set of technical specifications of the operating conditions of the wind power generation prototype analyzed in this article is summarized in the Table (7).

Table 7. Technical specifications for the operating scenarios.

Parameter	Value
DC motor power range	$v_{cc} = 0 - 50V, i_{cc} = 0 - 6A$
VSI CC bus voltage	$v_{bar} = 100$ V
DC-link capacitors	$C = 4700\ \mu F$
filter inductors L	$l_c = 500\ \mu F$
EFR magnetizing inductance	$l_m = 0.22$ H
Voltage in the generator field winding	$v_f = 0 - 7.0$ V
Current in the generator field winding	$i_f = 0 - 4.5$ A
DAQ - electrical signal sampling	1 kHz
DAQ - mechanical velocity signal sampling	5 Hz
Resistive load per phase	$P_r = 200$ W

5.2. Empty Synchronous Generator Traction

5.2.1. Open-Loop Speed Regulation

In order to analyze the prototype performance in an open loop, a test of 28 s is presented in Figure 9. Initially, a 15 Hz signal is synthesized by the reference voltages from the VSI and causes the rotor to reach an average velocity of 932 rpm, as shown in Figure 9a. At instant τ_1, the synchronous generator field circuit is triggered with v_f = 7.0 V and i_f = 4.5 A in the field circuit and gives rise to the rms empty voltages equivalent to 105 V per phase, as can be seen in Figure 9b. The frequency generator operating time is 31 Hz and is very far from its nominal value. Although negligible in most applications, the counter-torque on the crankshaft generator operating on empty cannot be disregarded for the prototype, as it is possible to identify a smooth deceleration in the rotor velocity due to the counter-torque that appears on the axis of rotation, even with no load coupled to the generator terminals. At the instant τ_2, the DC motor is gradually activated to reach a velocity equivalent to 310.4 rpm. This velocity is imposed on the EFR through armature, as illustrated in Figure 9c. The rotor perceives the velocity in armature and accelerates to the average value of 1224 rpm.

Preprints (www.preprints.org) | NOT PEER-REVIEWED | Posted: 21 June 2022 doi:10.20944/preprints202206.0277.v1

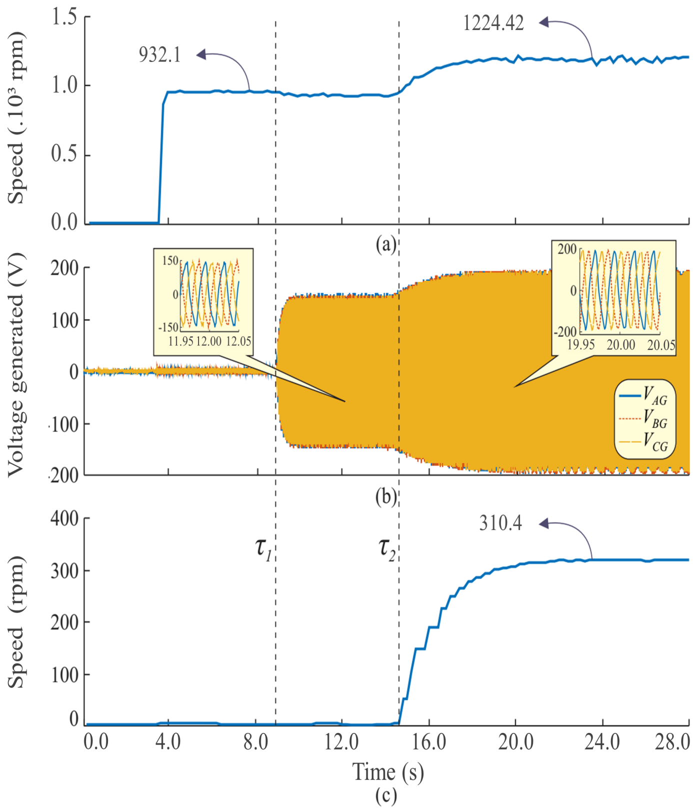

Figure 9. Open-loop speed gain analysis with illustration of the performance of the (a) rotor speed, (b) the generator output voltages and (c) armature speed.

After stabilizing the armature velocity at a value close to 30% of rotor speed, the voltages available at the synchronous generator terminals have a value effective and electrical frequency equivalent to 138 V and 40.8 Hz, respectively, which represent an increase, also respectively, of 21% and 31.6% with the initial performance. With this, the percentage value of armature velocity is transferred in the same proportion to rotor, taking the same field current in the generator synchronous. Although this essay is important for the velocity gains illustration mechanics that EFR can provide, it illustrates the shortcoming of loop control open when applied to the prototype. It is clear that, due to the increase in the value effective and electrical frequency of the generator output voltages, electrical loads may suffer irreparable damage. This occurs because consumers are characterized by the possession of devices that operate within a very narrow tolerance range of voltage variations and electrical frequency. It is worth noting that the performance observed with the velocity regulation with scalar control is similar to that obtained in the simulation analyzes of the elementary model of the EFR, discussed in the section 3. Thus, based on the impossibility of maintaining the rotor velocity at a constant value in an open loop, this control strategy will not be present in the subsequent analyses from a quality point of view of electric energy delivered to the load.

5.2.2. Speed Regulation by FOC Control

The guarantee of voltage and frequency stability at the output of the generator that supplies a resistive load is only possible by eliminating rotor speed variations. For this purpose, rotor-flux-oriented control is performed, as discussed in the section (4). The gains of the controllers and the most relevant information concerning the current loops in the synchronous reference, magnetic flux, and velocity regulation rotor can be observed in the Tables (8), (9) and (10), respectively. The criteria adopted for generator traction at no load were the stabilization time at 2% (t_s) less than 30 s and the overshoot coefficient (μ_p) less

Preprints (www.preprints.org) | NOT PEER-REVIEWED | Posted: 21 June 2022 doi:10.20944/preprints202206.0277.v1

than to 5%. They emphasized that the dimensioning of the controller gains goes through a process of fine-tuning to compensate for non-modeled nonlinearities.

Table 8. Current regulator parameters in the synchronous reference $R_{idq}(s)$.

Parameters $R_{idq}(s)$			
$k_{p_{id}}$	25.0	$k_{p_{iq}}$	60.0
$k_{i_{id}}$	20.0	$k_{i_{iq}}$	25.0

Table 9. Rotor flux regulator parameters $R_{\phi}(s)$.

	Parameters $R_{\phi}(s)$
ϕ^*_{ref}	0.8 W_b
$k_{p_{\phi}}$	3.0
$k_{i_{\phi}}$	3.5

Table 10. Speed regulation parameters $R_w(s)$.

	Parameters $R_w(s)$
w^*_{ref}	188.5 rad/s
k_{p_w}	1.3
k_{i_w}	2.0

Prototype performance with conventional speed regulation is illustrated in Figure 10. The imposition of a step-type reference gives rise to a transient response in the rotor velocity control, as seen in Figure 10a. Still, that the supersign reaches values of the order of 1935.5 rpm (or a μ_p = 7.53%), the time stabilization achieved is much lower than expected. The observed steady-state error is equivalent to 0.078% and can be considered null, even considering oscillations in the acquisition of rotor speed values. The high value of (μ_p) is due to an empirically detected lower limit for the value of $k_{p_{iq}}$ that when below the value used, for that operating point, considerably reduces the overshoot but does not reach the desired reference and accumulates relevant steady-state error values. The overshoot dynamics caused by the EFR start transient is reflected in the terminal voltages of the synchronous generator, according to Figure 10b. With an effective value close to 140 V and a frequency of 60.04 Hz. In Figure 10c, it is possible to observe the activation of the DC motor, which moves the armature. For the evaluated period, two-rotor speed profiles are imposed at different times to have 400 and 800 rpm in the armature. The conventional speed regulation can keep the rotor speed throughout the entire experiment, even with the insertion of movement in the armature. From a speed multiplication point of view, when the armature is at 393.1 rpm, the gain is approximately 4.58, while for a armature rotation at 800.2 rpm, the gain is about 2.25. This velocity gain occurs without any disturbance being transferred to the terminal voltage of the synchronous generator, which is kept stable throughout the armature transient, as can be identified in the fundamental cycles of the voltage generated in the period of 100 s.

Preprints (www.preprints.org) | NOT PEER-REVIEWED | Posted: 21 June 2022 doi:10.20944/preprints202206.0277.v1

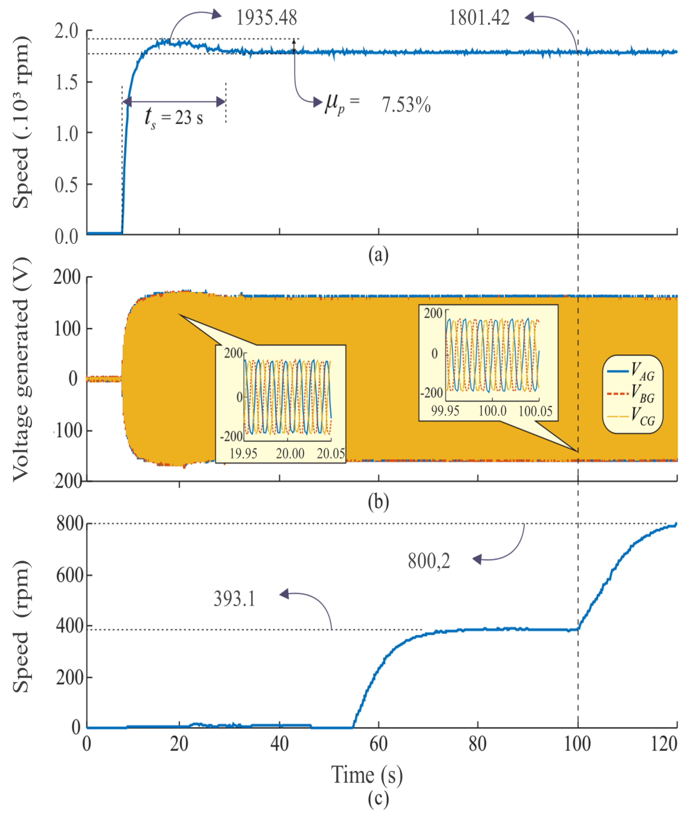

Figure 10. Analysis of velocity gain by conventional regulation with illustration of the performance (a) rotor speed, (b) the generator output voltages, (c) speed armature.

5.2.3. Speed Regulation by Fuzzy Control

The experimental validation of the behavior of the Fuzzy controller is performed using a test similar to the test with conventional control and with the objectives kept the same: voltage and electrical frequency stability. The performance criteria taken as a reference are also ts less than 30 s and admission of a overshoot value that does not exceed the value of 5% of the reference imposed on the system. For the screen experiment, the field circuit of the synchronous generator is fed with v_f = 5.9 V and i_f = 3.6 A. The gains associated with the inference rules defined according to the equation (12) are summarized in the Table (11). Although tuning the fuzzy controller does not need to take into account specific parameters of the plant model to be controlled, the gains obtained for the conventional regulation served as a starting point for the adjustment of the fuzzy controller gains. After some initial tests, it was empirically noticed that much smaller gains than those employed in conventional regulation already reached the performance criteria.

Table 11. Fuzzy controller gains after empirical adequacy.

$K_{p1,2,3}$	0.2	$K_{p4,5,6}$	0.7	K_{p7}	2.5	K_{p8}	2.9	K_{p9}	2.5
$K_{p1,2,3}$	0.5	$K_{p4,5,6}$	1.1	K_{p7}	8.0	K_{p8}	12.5	K_{p9}	4.0

The prototype performance with speed regulation by fuzzy control is illustrated in Figure 11. The rotor velocity response of the EFR when enforcement occurs of the same speed step of 1800 rpm can be seen in Figure 11a. The stabilization time achieved was approximately seven times shorter than that established as a reference criterion. Contrary to what is expected for a reduction in t_s with conventional speed regulation, the rotor dynamic response has no overshoot and stabilizes at an average value of 1794.2 rpm, which is equivalent to a steady-state error of 0.32%, which can also be considered null. The overshoot absence in the rotor velocity due to the fuzzy speed regulation makes

 doi:10.20944/preprints202206.0277.v1

the EFR start-up smooth, and the terminal voltages of the synchronous generator do not experience any level of transient overvoltage, as shown in Figure 11b. During steady-state, the effective value and frequency of the voltages generated are equivalent to 139.1V and 59.81Hz, respectively.

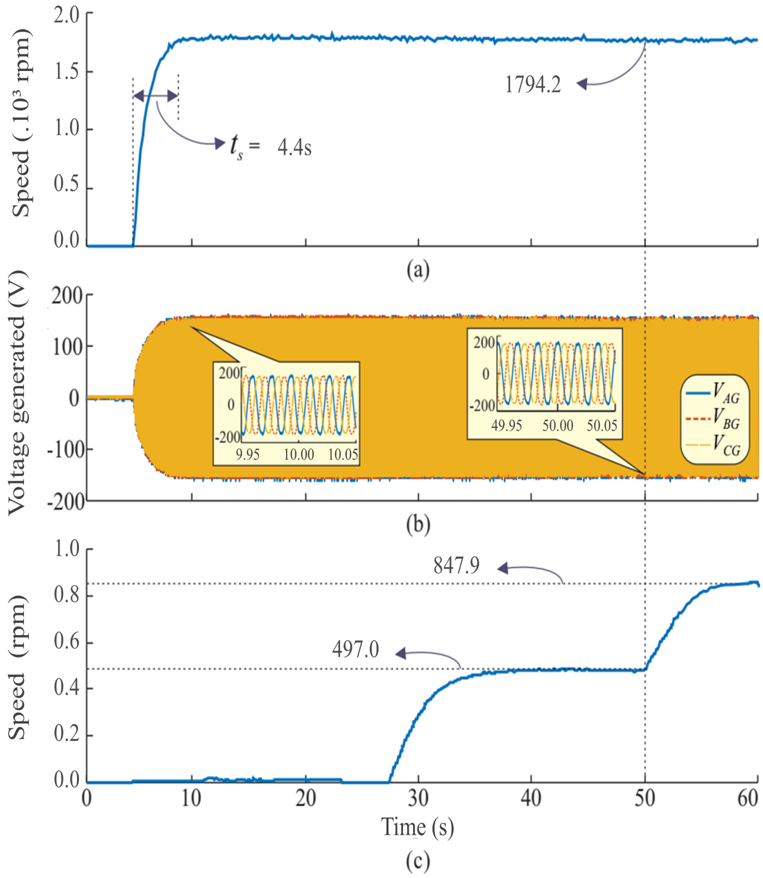

Figure 11. Analysis of speed gain by Fuzzy regulation with illustration performance of (a) rotor speed, (b) the generator output voltages and (c) armature speed.

The DC motor drive that moves the armature can be seen in Figure 11c. For the evaluated period, two-rotor velocity profiles are imposed at different times to have 497.0 and 847.9 rpm in the armature. The fuzzy speed regulation can also keep the velocity constant of rotor throughout the experiment, even with the insertion of movement in the armature. For this test, when the armature is at 497.0 rpm, the gain is approximately 3.61, while for a armature rotation at 847.9 rpm, the gain is about 2.12. This speed gain also occurs in parallel with maintaining voltage stability and frequency available at the synchronous generator terminals.

5.2.4. Performance Indices

According to [19], the performance index is a measure quantitative performance of the system and chosen in such a way that it emphasizes specifications system important. A commonly used performance index is the integral of the absolute error (IAE, Integral of the Absolute magnitude of the Error), which is defined by:

$$IAE = \int_0^T |e(t)|dt \tag{13}$$

Preprints (www.preprints.org) | NOT PEER-REVIEWED | Posted: 21 June 2022 doi:10.20944/preprints202206.0277.v1

To avoid the influence of a large input error signal during systems with a step reference, In [19] propose the use of the index of the integral time multiplied by absolute error (ITAE) defined by:

$$ITAE = \int_0^T t|e(t)|dt \tag{14}$$

The ITAE provides better selectivity of performance indices, as the value minimum of the integral is easily distinguished while the system parameters are changed.

5.2.5. Comparison of Control Strategies through Performance Indicators

For the graphical analysis and the analysis of transient regime parameters, the indices controller performance are evaluated in accordance with the equations (13) and (14) , in the section (5.2.4). The indices values calculated in the synchronous generator traction scenario empty, with both closed-loop control strategies, are summarized in the Table (12).

Table 12. Comparison of performance indicators for control strategies.

Indicator	Conventional	Fuzzy	Reduction (%)
IAE	$9.5084e+04$	$5.8363e+04$	38.60
ITAE	$7.4050e+05$	$4.2112e+05$	43.13

According to Table(12), the conventional speed regulation obtained higher values for the accumulated error and for the error in relation to the time when compared to fuzzy regulation indices. The absence of overshoot, together with the reduced t_s due to fuzzy control, it causes a reduction average of 40.8% of the performance indicators in relation to the conventional control.

5.3. Synchronous Generator Traction under Load

For evaluating the power flow of the power generation prototype based on the EFR, the two closed-loop control strategies are used for the traction of the synchronous generator when it supplies constant power to the resistive load of 200 W per phase. Under these conditions, the field circuit of the synchronous generator is driven with v_f = 3.15 V and i_f = 1.79 A. The operating point chosen for the analysis had to change. Based on a test build, the operating speed of the synchronous generator has been reduced to 1200 rpm. Furthermore, for the purposes of this analysis, only the steady-state will be considered for the following calculations. In these operating scenarios, the influences of the armature speed variation through driving force, emulated by the DC motor.

5.3.1. Velocity Regulation by FOC Control

For the evaluation of the electrical power transfer performance of the prototype with conventional rotor speed regulation, a test of 280 s is illustrated in Figure 12. The controller gains are the same as used in the section (5.2.2). The armature speed variation is performed in four distinct sectors identified by A, B, C and D, with values of 300, 580, 860 and 1080 rpm, respectively, and can be observed in Figure 12a. A detailed exploration of sector A is carried out based on the Figures from 12b to 12g. The voltages and electrical currents supplied by the VSI to the EFR can be observed in Figures 12b and 12c, respectively. Due to the constructive aspects of the EFR, there is an evident imbalance between its phases, with an average RMS value per voltage phase and current of 60.0V and 12.9A, respectively. The profile of voltages and currents supplied by the synchronous generator to the resistive load can be analyzed in Figures 12d and 12e, respectively. Again, with operation at a speed value far from the rated value, the maximum voltages generated are also lower than expected for the rated performance of the synchronous generator, with maximum values, on average, of 100V per phase. With the objective of mitigating the influences of oscillations arising from the speed variation imposed on the armature, the evaluation of the power flow is

Preprints (www.preprints.org) | NOT PEER-REVIEWED | Posted: 21 June 2022 doi:10.20944/preprints202206.0277.v1

carried out in a period of 10 s, as illustrated in Figure 12f. In this figure, there are the active power curves involved in the system elements. Throughout the analysis, it is possible to observe an average power of approximately 1.0 kW consumed by the EFR, from 600 W by the resistive load, while the DC motor provides something over 300 W to armature. It is worth noting that the active power consumed by the EFR is measured at the output of the three-phase VSI and therefore does not represent the mechanical power available at the tip of the rotor axis. For power flow assessment, the two driving forces emulated by the DC motor and the VSI that powers the EFR are considered positive power flow. On the other hand, resistive load consumption is defined as a negative power flow in the energy balance equation.

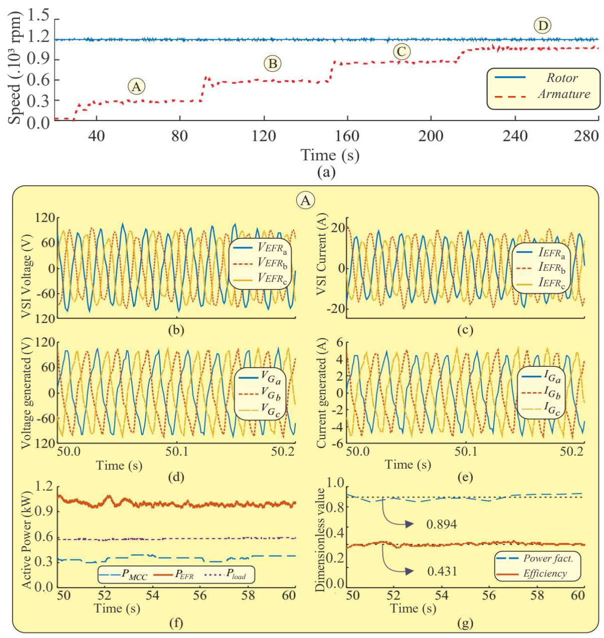

Figure 12. Power flow analysis with conventional speed regulation with illustration of (a) rotor and armature profiles, (b) voltages and (c) currents consumed by EFR, (d) voltages (e) currents consumed by the resistive load, (f) electrical power of the devices and g) EFR power factor and prototype global efficiency.

System efficiency is estimated based on the percentage of available power at the output of the system in relation to the amount of input power and is illustrated in 12f with the EFR power factor in the same period considered for Figure 12g. The system efficiency reaches an average value of 43.1% in the evaluated period, while the power factor reaches the value of 0.894 inductive. The existence of a factor powerless than unity occurs due to the EFR synchronous field maintenance.

5.3.2. Power flow analysis with fuzzy speed regulation

For the evaluation of the electrical power transfer performance of the prototype with rotor speed Fuzzy regulation, a slightly shorter test is analyzed, totaling 120 s, and is illustrated in Figure 13 The associated gains of the Fuzzy controller are the same as those used in the section (5.2.3), and the generator excitation circuit synchronous remains unchanged. For this test, the armature speed variation follows the same sectoral profile defined previously and can be seen in Figure 13a, with a specific detail of sector A that is

Preprints (www.preprints.org) | NOT PEER-REVIEWED | Posted: 21 June 2022 doi:10.20944/preprints202206.0277.v1

illustrated in the Figures from 13b to 13g. The voltages and electrical currents supplied by the VSI to the EFR can be observed in the Figures 13b and 13c, respectively. Due to the constructive aspects of the EFR, with an average RMS value per voltage phase and current of 58.0 V and 13.0 A, respectively, which are very similar values to those obtained for conventional speed regulation. The profile of voltages and currents supplied by the synchronous generator to the resistive load can be analyzed in Figures 13d and 13e, respectively. For the operation of EFR's rotor with a speed value lower than the rated value, the maximum voltages generated are also lower than expected for the nominal performance of the synchronous generator, with maximum values, on average, of 99 V per phase. With the objective of mitigating the influences of oscillations arising from the speed variation imposed on the armature, the evaluation of the power flow is carried out in a period of consecutive 5 seconds, as illustrated in Figure 13f. Over the evaluation time, it is possible to observe an average power slightly less than 1.0 kW consumed by the EFR, of 600 W by the resistive load, while the DC motor provides, on average, 330 W to the armature. The efficiency of the system is illustrated in 13g together with the power factor of the EFR in the same period considered for the analysis of the individual powers of Figure 13f.

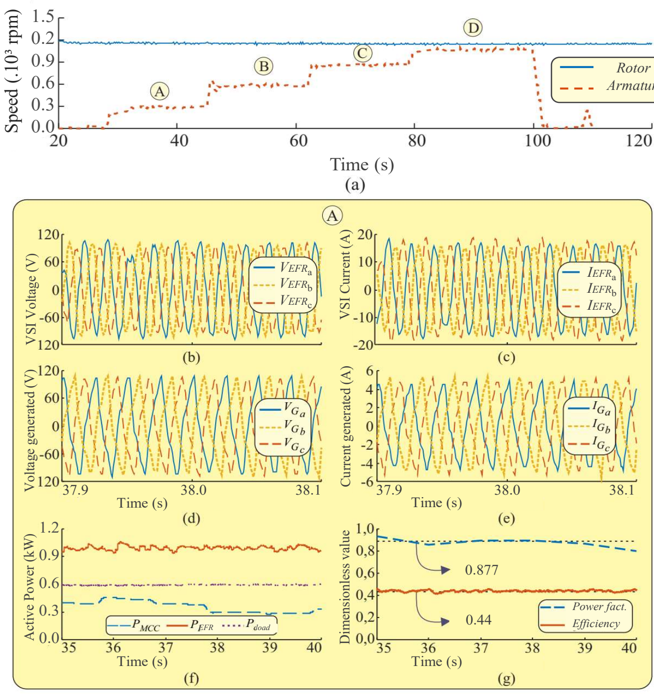

Figure 13. Power flow analysis with fuzzy speed regulation with illustration of the (a) rotor and armature profiles, (b) Voltage and (c) currents consumed by the EFR, (d) Voltage, (e) currents drawn by the resistive load, (f) electrical power of devices a, and (g) EFR power factor and overall prototype efficiency.

The system efficiency reaches an average value of 44.0% in the evaluated period, while the power factor reaches the value of 0.877 inductive. Thus, there is an increase in 0.9% concerning the average efficiency obtained by conventional speed regulation and a reduction in the magnitude of the power factor, still inductive, by 0.017.

6. Conclusions

The article proposes a contribution to the control strategy applied to the prototype power generation based on EFR, making the theoretical study difficult through computer simulations was proposed using the models of induction machines, which are widely known in the scientific community. In order to better identify the operating ranges of the prototype, several tests with load variation on the synchronous generator and wind emulation. For these scenarios, the fuzzy controller was compared with the conventional controller, proposed together with the creation of the EFR. In scenarios where the generator is idle, the speed regulation by the fuzzy controller presents the best performance in the transient regime when compared to the conventional regulation. This is due to the absence of overshoot in rotor, which allows a smooth start to the prototype and eliminates the need for a sequential start of the EFR, generator, and resistive load. Furthermore, the gains associated with the fuzzy controller to obtain this better performance are lower than those imposed by conventional regulation based on the PI controller. The fuzzy controller presented a regime error four times higher than the PI controllers for steady-state. However, this is not a demerit for the fuzzy due to the magnitudes of the errors obtained. An error of 0.32% can be considered zero for this application. Furthermore, for the evaluation of the controllers, there was a significant reduction in the IAE and ITAE indicators for fuzzy speed regulation. Thus, fuzzy regulation presents better applicability to the prototype concerning the current speed regulation. From the power flow point of view, the prototype's efficiency presents a tendency for efficiencies to decrease as the armature and rotor speed match. However, for the tests evaluated, the fuzzy regulation presented the advantage of providing a less accentuated reduction, characterizing robustness with the velocity multiplication compared to the conventional controller.

Based on the results obtained in this study and on the limitations found in the prototype generation with the EFR, the following proposals for future works are suggested: 1) Study ways of sizing machines to obtain an optimization via the good choice of the numbers of poles of the EFR and the generator; 2) Making a new generation prototype based on the new version of the EFR, with the necessary mechanical corrections; 3) Improvement of the fuzzy controller used, with greater quantity and profiles of membership functions being applied; 4) implementation of flux-slip-based control strategies rotor; 5) Implementation of control strategies that guarantee operation with a factor of the EFR's nominal power.

Author Contributions: E. F. N., R. P. and A. S. conceived and designed the study; D. C., T. do N. and R. P., methodology ; R. P. , T. do N. and E. F. N. performed the simulations and experiments; E. V., D. C., R. P. and A. S. reviewed the manuscript and provided valuable suggestions; D. C. T. do N., R. P. and E. F. N. wrote the paper; supervision, A. S.

Funding: This research was funded in part by the Coordenação de Aperfeiçoamento de Pessoal de Nível Superior—Brasil (CAPES)—Finance Code 001 and Conselho Nacional de Desenvolvimento Científico e Tecnológico (CNPq).

Conflicts of Interest: The authors declare no conflicts of interest.

Abbreviations

The following abbreviations are used in this manuscript:

AI	Artificial Intelligence
PCC	Point of Common Coupling
COMSOL	COMSOL Multphysics Simulation Software
DC	Direct Current
DFIG	Doubly-Fed Induction Generator
DTC	Direct Torque Control
EFR	Electromagnetic Frequency Regulator
EPS	Electrical Power System
FOC	Field Oriented Control
IAE	Integral of the Absolute magnitude of the Error
ITAE	Integral of Time multiplied by the Absolute Error
PI	Proportional-Integral
PID	Proportional-Integral-Derivative
PMSG	Permanent Magnet Synchronous Generator
RES	Renewable Energy Sources
RLM	Root Locus Method
V/F	Voltage-Frequency
VSI	Voltage Source Inverter

References

1. Polinder, H.; Ferreira, J. A.; Jensen, B. B.; Abrahamsen, A. B.; Atallah, K.; Mcmahon, R. A. Trends in wind turbine generator systems. *IEEE Journal of Emerging and Selected Topics in Power Electronics* **2013** , *1(3)*, 174–185.
2. Mckenna, R.; Leye, P. O. v.d.; Fichtner, W. Key challenges and prospects for large wind turbines. *Renewable and Sustainable Energy Reviews* **2016** , *53*, 1212–1221.
3. Alhmoud, L.; Wang, B. A review of the state-of-the-art in wind-energy reliability analysis. *Renewable and Sustainable Energy Reviews* **2018** , *81*, 1643–1651.
4. Azevedo, H. D. M.; Araújo, A. M.; Bouchonneau, N. A review of wind turbine bearing condition monitoring: State of the art and challenges.*Renewable and Sustainable Energy Reviews* **2016** , *56*, 368–379.
5. Ribrant, J. ; L. M. Bertling, L. M. Survey of Failures in Wind Power Systems With Focus on Swedish Wind Power Plants During 1997–2005. in *IEEE Transactions on Energy Conversion* **2007**, *22(1)*, 167–173.
6. Perez, J. M. P.; Marquez, F. P. G.; Tobias, A.; Papaelias, M. Wind turbine reliability analysis. *Renewable and Sustainable Energy Reviews* **2013** , *23*, 463–472.
7. IEEE Standard for Interconnection and Interoperability of Distributed Energy Resources with Associated Electric Power Systems Interfaces. *IEEE Std 1547-2018 (Revision of IEEE Std 1547-2003)* **2018** , 1–138.
8. Vitor Silva, P. ; Ferreira Pinheiro, R. ; Ortiz Salazar, A ; Pereira do Santos Junior, L. ; Cesar de Azevedo, C. A Proposal for a New Wind Turbine Topology Using an Electromagnetic Frequency Regulator. *IEEE Latin America Transactions* **2015**, *13(4)*, 989–997.
9. Silva, P. V. : Pinheiro, R. F. ; Salazar, A. O. ; Fernandes, J. D. Performance analysis of a new system for speed control in wind turbines. *Renewable energy & power quality journal* **2015** , *1*, 455–460.
10. Silva, P. V. ; Pinheiro, R. F. ; Salazar, A. O. Júnior, L. P. S. ; Fernandes, J. D. A New System for Speed Control in Wind Turbines using the Electromagnetic Frequency Regulator. *Eletrônica de Potência* **2015** , *20*, 254–262.
11. Ramos, T.; Júnior, M.M.; Pinheiro, R.; Medeiros, A. Slip Control of a Squirrel Cage Induction Generator Driven by an Electromagnetic Frequency Regulator to Achieve the Maximum Power Point Tracking. *Energies* **2019**, *12*, 2100.
12. Da Silva, J. C. L. ; Ramos, T. ; Junior, M. F. M. Modeling and Harmonic Impact Mitigation of Grid-Connected SCIG Driven by an Electromagnetic Frequency Regulator. *Energies* **2021**, *14(15)*, 4524–4524.
13. Jacobina, C. B. ; Lima, A. M. N. Estratégias de Controle Para Sistemas de Acionamento Com Máquina Assíncrona. *SBA Controle & Automação* **1996** , *7(1)*, 15–28.
14. Do Nascimento, T. F. ; Nunes, E. A. F. ; Salazar, A. O. Modeling and Controllers Design for an Electromagnetic Frequency Regulator Applied to Wind Systems. 2021 Brazilian Power Electronics Conference (COBEP), 7 and 10 November 2021, pp. 1-8.
15. Do Nascimento, T. F. ; Nunes, E. A. F. ; Villarreal, E. R. L. ; Pinheiro, R. F. ; Salazar, A. O. Performance Analysis of an Electromagnetic Frequency Regulator under Parametric Variations for Wind System Applications. *Energies* **2022**, *15 (2873)*, 1–27. https://doi.org/10.3390/ en15082873
16. Pessoa, G. A. P. C.; Pinheiro, R. F.; Nunes, E. A. de F.; Pinheiro, R. X. de O. Sistema supervisório para motores de indução trifásicos. Congresso Brasileiro de Extensão Universitária- CBEU, 2018.
17. Simoes, M. G.; Shaw, I. S. Controle e modelagem fuzzy. São Paulo: Blusher, 2007.
18. Araújo, F. M. U. ; Cavalcante, M. S. F. F. ; Vasconcellos, B. S. de ; Mendes, W. R. Comparison of fuzzy type-2 and conventional fuzzy controllers tuned by ant colony optimization. 24th ABCM International Congress of Mechanical Engineering), 2017. p. 9.
19. Nise, N. S. Control Systems Engineering, 6rd ed., John Wiley & Sons, Inc., USA, 2011.